

tainty are taken from an envelope of cross section predictions using different PDF sets and factorisation and renormalisation scales, as described in Ref. [69].

Direct \tilde{t}_2 pair production is studied using a simplified model, where all SUSY particles are decoupled except for the \tilde{t}_2 , \tilde{t}_1 and $\tilde{\chi}_1^0$, assumed to be the LSP. The only decays included in this model are $\tilde{t}_2 \rightarrow Z\tilde{t}_1$ and $\tilde{t}_1 \rightarrow t\tilde{\chi}_1^0$. The mass of the top quark is fixed at 172.5 GeV. The mass difference between the lighter stop and the neutralino is set to 180 GeV, a region not excluded by previous searches [21], and signal samples are generated varying the masses of the \tilde{t}_2 and $\tilde{\chi}_1^0$. In addition, dedicated samples also including the $\tilde{t}_2 \rightarrow h\tilde{t}_1$ and $\tilde{t}_2 \rightarrow t\tilde{\chi}_1^0$ decay modes are used to interpret the results as a function of the \tilde{t}_2 branching ratios. Simulated samples corresponding to direct \tilde{t}_1 pair production for values of $m_{\tilde{t}_1} = m_{\tilde{\chi}_1^0} + 180$ GeV are also used in the analysis.

For the natural GMSB scenario, a very similar model to that of Ref. [34] is considered, with the Higgs boson assumed to be SM-like and with the mass set at 126 GeV, in agreement with the observation of a Higgs boson at the LHC [70, 71], and with $\tan \beta$, the ratio of the vacuum expectation value of the two neutral Higgs doublets of the MSSM, set to 5. The masses of the first and second generation squarks and gluinos (superpartners of the gluons) are above 5 TeV, and maximal mixing between the squark eigenstates is assumed for \tilde{t}_1 . Only \tilde{t}_1 pair production is considered. $\tilde{\chi}_1^0$, $\tilde{\chi}_2^0$ and $\tilde{\chi}_1^\pm$ are assumed to be predominantly higgsino states. Hence, if $\tilde{\chi}_2^0$ or $\tilde{\chi}_1^\pm$ are produced in a decay chain, they decay to $\tilde{\chi}_1^0$ promptly with soft accompanying fermions. The branching fractions of the \tilde{t}_1 and higgsino decays are predicted by the model. If $m_{\tilde{t}_1} < m_t + m_{\tilde{\chi}_1^0}$, \tilde{t}_1 decays via $\tilde{t}_1 \rightarrow b\tilde{\chi}_1^\pm$ exclusively, while if $m_{\tilde{t}_1} > m_t + m_{\tilde{\chi}_1^0}$, \tilde{t}_1 may also decay with similar probability via $\tilde{t}_1 \rightarrow t\tilde{\chi}_1^0$ (or $t\tilde{\chi}_2^0$). For the model parameters considered, the $\tilde{\chi}_1^0$ predominantly decays to $Z\tilde{G}$ with branching ratios typically above 70 %. Signal samples are generated varying the \tilde{t}_1 and $\tilde{\chi}_1^0$ masses.

4 Object identification and event selection

After the application of beam, detector and data quality requirements, the total luminosity considered in this analysis corresponds to 20.3 fb^{-1} . The uncertainty on the integrated luminosity is $\pm 2.8 \%$. It is derived, following the same methodology as that detailed in Ref. [72], from a preliminary calibration of the luminosity scale derived from beam-separation scans performed in November 2012.

Events are selected if they pass the single electron or muon triggers; these are fully efficient for lepton $p_T > 25$ GeV. The presence of at least one primary vertex, with at least five tracks with $p_T > 0.4$ GeV associated to it, is required. In order to optimize the analysis and to perform data-driven

background estimations, two categories of jets, electrons, muons and photons are defined: “candidate” and “signal” (with tighter selection criteria).

Jets are reconstructed from three-dimensional calorimeter energy clusters by using the anti- k_t algorithm [73] with a radius parameter of 0.4. Jet energies are corrected [74] for detector inhomogeneities, the non-compensating nature of the calorimeter, and the impact of multiple overlapping pp interactions, using factors derived from test beam, cosmic ray and pp collision data and from a detailed GEANT4 detector simulation. Events with any jet that fails the jet quality criteria designed to remove noise and non-collision backgrounds [74] are rejected. Jet candidates are required to have $p_T > 20$ GeV and $|\eta| < 2.8$. Jets labelled as signal jets are further required to have $p_T > 30$ GeV and, for those with $p_T < 50$ GeV and $|\eta| < 2.4$, the jet vertex fraction, defined as the fraction of the sum of the p_T of the tracks associated with the jet and matched to the selected primary vertex, normalised by the sum of the p_T of all tracks associated with the jet, is required to be larger than 25 %.

Identification of jets containing b -quarks (b -tagging) is performed with a dedicated algorithm based on a neural-network approach which uses the output weights of several b -tagging algorithms [75] as input. A requirement is chosen corresponding to a 60 % average efficiency obtained for b -jets in simulated $t\bar{t}$ events. The rejection factors for mis-tagging light quark jets, c -quark jets and τ leptons in simulated SM $t\bar{t}$ events are approximately 600, 8 and 24, respectively. Signal jets with $|\eta| < 2.5$ which satisfy this b -tagging requirement are identified as b -jets. To compensate for differences between data and MC simulation in the b -tagging efficiencies and mis-tag rates, correction factors derived from different methods, such as the use of the p_T of muons relative to the axis of the jet [76] and a dedicated study in $t\bar{t}$ dominated regions [77], are applied to the simulated samples. A sample of D^{*+} mesons is used for mis-tag rates of c -jets [78] and inclusive jet samples for mis-tag rates of a jet which does not originate from a b - or c -quark [79].

Electron candidates must satisfy the “medium” selection criteria described in Ref. [80], re-optimised for 2012 data, and are required to fulfil $p_T > 10$ GeV and $|\eta| < 2.47$. Signal electrons must pass the previous requirements and also need to be isolated, i.e. the scalar sum of the p_T of charged-particle tracks within a cone of radius $\Delta R = 0.3$ around the candidate excluding its own track must be less than 16 % of the electron p_T . In addition, a longitudinal impact parameter requirement of $|z_0 \sin \theta| < 0.4$ mm is applied to signal electrons. The track parameter z_0 is defined with respect to the reconstructed primary vertex.

Muon candidates are required to have $p_T > 10$ GeV, $|\eta| < 2.4$ and are identified by matching an extrapolated inner detector track and one or more track segments in the muon spectrometer [81]. Signal muons are then required to

be isolated, i.e. the scalar sum of the p_T of charged-particle tracks within a cone of radius $\Delta R = 0.3$ around the muon candidate excluding its own track must be less than 12 % of the muon p_T . In addition, a longitudinal impact parameter requirement of $|z_0 \sin \theta| < 0.4$ mm is applied to signal muons.

A signal lepton with p_T larger than 25 GeV is required to match the one that triggered the event such that the efficiency of the trigger is p_T independent. The MC events are corrected to account for minor differences in the lepton trigger, reconstruction and identification efficiencies between data and MC simulation [80,81].

To resolve ambiguities between reconstructed jets and leptons, jet candidates within a distance of $\Delta R = 0.2$ of an electron candidate are rejected. Any electron or muon candidate within a distance of $\Delta R = 0.4$ of any remaining jet candidate is also rejected. To suppress the rare case where two distinct tracks are mistakenly associated with one calorimeter energy cluster forming two electron candidates, if two electron candidates are found within a distance $\Delta R = 0.1$, the one with smaller transverse momentum is rejected. Finally, to suppress muon bremsstrahlung leading to an incorrect measurement of the transverse momentum, if an electron candidate and a muon candidate are within $\Delta R = 0.1$, both are rejected.

Photons are used only for the $Z + \text{jets}$ estimation in the two-lepton signal regions described in Sect. 5 and the overlap removal between photons and jets described below is performed only in this case. Photon candidates are required to have $p_T > 25$ GeV, $|\eta| < 2.47$ and must satisfy the “tight” selection criteria described in Ref. [82]. Signal photons are further required to be isolated, i.e. the scalar sum of transverse energy deposition in the calorimeter observed within a cone

of radius $\Delta R = 0.4$ around the photon candidate excluding its own energy deposition in the calorimeter must be less than 4 GeV. To resolve overlaps between reconstructed jets and photons, jet candidates within a distance of $\Delta R = 0.2$ of a photon candidate are rejected.

The calculation of the missing transverse momentum, where its magnitude is referred to as E_T^{miss} [83], is based on the vector sum of the transverse momenta of all electron, muon and jet candidates, as well as photons with $p_T > 10$ GeV and calibrated calorimeter energy clusters with $|\eta| < 4.9$ not associated with these objects. Clusters associated with electrons, photons and jets make use of the calibrations of these objects. For jets, the calibration includes the pile-up correction described above, whilst the jet vertex fraction requirement is not considered when selecting jet candidates for computing the E_T^{miss} . Clusters not associated with these objects are calibrated using both calorimeter and tracker information [83].

Five signal regions (SRs) are defined in the analysis aiming at final states with a Z boson, b -jets, significant E_T^{miss} and possibly additional leptons, as summarised in Table 1. They are characterised by the number of leptons (electrons or muons) required in the final state. For the two-lepton SRs (indicated as SR2A, SR2B and SR2C), events with exactly two leptons are selected, with the p_T of the leading one required to be larger than 25 GeV. They are required to be signal leptons and form a SFOS pair with invariant mass ($m_{\ell\ell}$) within 5 GeV or 10 GeV of the Z -boson mass. At least one b -jet is required. SR2A and SR2B are optimised for the small $m_{\tilde{t}_1} - m_{\tilde{\chi}_1^0}$ region of the natural GMSB model where low jet multiplicity is expected, whilst SR2C is optimised for the large $m_{\tilde{t}_1} - m_{\tilde{\chi}_1^0}$ region where the jet multiplicity is

Table 1 Summary of the event selection in the signal and $t\bar{t}$ background control regions used in the analysis. The variables used are the number of leptons (N^{leptons}), the p_T of the leading lepton ($p_T(\ell_1)$), the dilepton flavour (SF: same-flavour; DF: different flavour), the dilepton invariant mass ($m_{\ell\ell}$), the number of b -jets ($N^{\text{b-jets}}$), the number of jets regardless of their flavour (N^{jets}), the p_T of the leading jet ($p_T(\text{jet}_1)$), the p_T of the N^{jets} -th jet required in each region ($p_T(\text{jet}_N)$), the missing transverse momentum (E_T^{miss}), the transverse momentum of the dilepton system ($p_T(\ell\ell)$), and the angular separation in the transverse plane between the leptons forming the SFOS pair ($\Delta\phi^{\ell\ell}$)

	SR2A	SR2B	SR2C	CR2A	CR2C	SR3A	SR3B
N^{leptons}	2	2	2	2	2	3	3
$p_T(\ell_1)$ (GeV)	>25	>25	>25	>25	>25	>40	>60
Dilepton flavour	SF	SF	SF	SF, DF	SF, DF	SF	SF
$ m_{\ell\ell} - m_Z $ (GeV)	<5	<10	<5	<50	<50	<10	<10
				>10 (SF)	>10 (SF)		
$N^{\text{b-jets}}$	≥ 1						
N^{jets}	3, 4	3, 4	≥ 5	3, 4	≥ 5	≥ 5	≥ 5
$p_T(\text{jet}_1)$ (GeV)	>30	>30	>30	>30	>30	>50	>40
$p_T(\text{jet}_N)$ (GeV)	>30	>30	>30	>30	>30	>30	>40
E_T^{miss} (GeV)	>160	>200	>160	>160	>120	>60	>60
$p_T(\ell\ell)$ (GeV)	>80	>160	>80	>80	>80	–	>75
$\Delta\phi^{\ell\ell}$ (rad)	<1.5	<1.5	<1.5	<1.5	<1.5	–	–

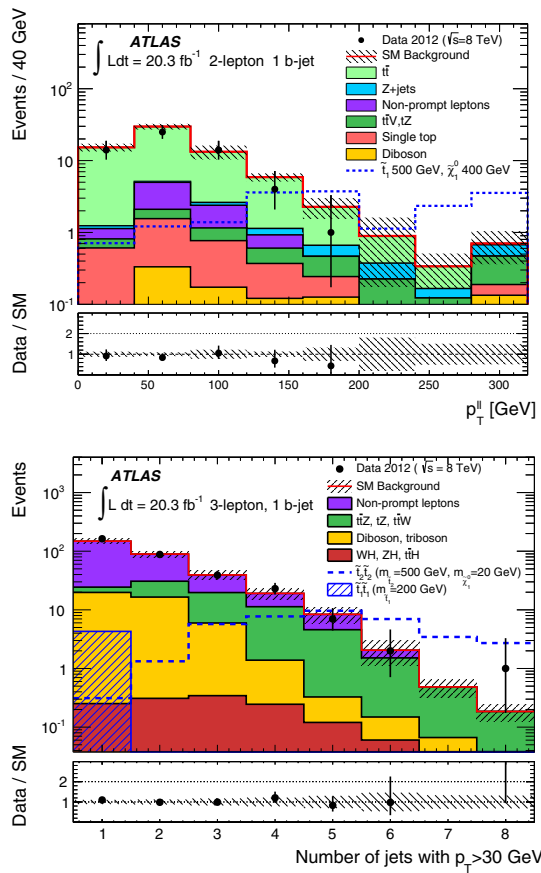


Fig. 1 Top, $p_T(\ell\ell)$ distributions in SR2A before the $p_T(\ell\ell) > 80$ GeV and $\Delta\phi^{\ell\ell} < 1.5$ selections. Bottom, number of signal jets with $p_T > 30$ GeV in events with 3 signal leptons after the lepton, $m_{\ell\ell}$ and b -jets selections in SR3A. Shaded bands denote the background statistical and systematic uncertainty. For illustration, distributions for selected signal points are also shown: the stop natural GMSB model with $m_{\tilde{t}_1} = 500$ GeV, $m_{\tilde{\chi}_1^0} = 400$ GeV (top) and the simplified model with $m_{\tilde{t}_2} = 500$ GeV, $m_{\tilde{t}_1} = 200$ GeV and $m_{\tilde{\chi}_1^0} = 20$ GeV for both direct \tilde{t}_2 and \tilde{t}_1 pair production (bottom). The last bin includes the histogram overflow

high. SR2A is optimised for a stop mass around 400 GeV and SR2B is for 600 GeV. Since the Z boson produced in stop signal events is typically boosted, the transverse momentum of the dilepton system, $p_T(\ell\ell)$, tends to be high while the azimuthal separation $\Delta\phi^{\ell\ell}$ tends to be low. This is illustrated by Fig. 1, which shows the $p_T(\ell\ell)$ distribution after the lepton, $m_{\ell\ell}$, jet and b -jet requirements in SR2A are applied. Requirements of $\Delta\phi^{\ell\ell}$ below 1.5 and $p_T(\ell\ell) > 80$ GeV or 160 GeV are therefore applied in the SRs. Finally, to enhance the signal contribution, typically with large E_T^{miss} due to the LSPs, $E_T^{\text{miss}} > 160$ GeV or 200 GeV is required depending on the targeted stop mass.

In the three-lepton SRs (indicated as SR3A and SR3B), at least three signal leptons with two of them forming an SFOS pair with invariant mass which is within 10 GeV of the Z boson mass are required. Two regions are optimised to

give good sensitivity in the direct \tilde{t}_2 pair production model for different $\tilde{t}_2 - \tilde{t}_1$ mass splittings. The SR3A is aimed at signal models with low mass splitting where the Z -boson is not boosted. The SR3B is optimised for high mass splitting where the Z -boson is boosted requiring a minimum p_T of the dilepton system of 75 GeV. A high- p_T leading lepton with a minimum p_T requirement of 40 GeV or 60 GeV for SR3A and SR3B respectively, and at least one b -jet are required to suppress the diboson background. The signal is expected to have higher jet multiplicity than the SM background, due to the presence of two top quarks and two Z bosons. This is illustrated by Fig. 1, which shows the jet multiplicity distribution after the lepton, $m_{\ell\ell}$, and b -jet requirements in SR3A are applied. Therefore at least five jets are required to increase the signal sensitivity.

5 Background estimation

Two main sources of background can be distinguished in this analysis: events containing at least one non-prompt or fake lepton (mainly production of multijets and W boson in association with jets in the two-lepton SRs, and production of top pairs and Z boson in association with jets in the three-lepton SRs) and events with two or three prompt leptons (mainly Z -jets and $t\bar{t}$ in the two-lepton SRs, and $t\bar{t}V$, tZ , diboson and triboson events in the three-lepton SRs).

Background from fake or non-prompt leptons

Fake leptons can originate from a misidentified light flavour quark or gluon jet (referred to as light flavour). Non-prompt leptons can originate from a semileptonic decay of a hadron containing a b - or c -quark (referred to as heavy flavour), or an electron from a photon conversion. The contribution from fake and non-prompt leptons is estimated from data with a matrix method similar to that described in Refs. [84, 85]. In order to perform the matrix method, two types of lepton identification criteria are defined: “tight”, corresponding to the signal lepton criteria described in Sect. 4, and “loose”, corresponding to candidate leptons. To increase the available statistics, muons within a $0.2 < \Delta R < 0.4$ distance from jets are also considered as loose muons in the method if the scalar sum of p_T of charged-particle tracks within a cone of radius $\Delta R = 0.3$ around the muon candidate excluding its own track is less than 30 % of the muon p_T . The matrix method relates the number of events containing fake or non-prompt leptons to the number of observed events with tight or loose leptons using the probability for loose prompt, fake or non-prompt leptons to pass the tight criteria. The probability for loose prompt leptons to pass the tight selection criteria is obtained using a $Z \rightarrow \ell\ell$ data sample and is modelled as a function of the lepton p_T . The probability for

erated. The pseudo-data sample is then normalised to data in the $E_T^{\text{miss}} < 80 \text{ GeV}$ region, after subtracting other SM background sources estimated by MC for real two lepton events and by the data-driven method for events with non-prompt leptons. Their contribution is less than 10 %. The jet energy resolution smearing function ($p_T^{\text{reco}}/p_T^{\text{truth}}$) is initially obtained from multijet MC simulation, where p_T^{reco} is the transverse momentum of the reconstructed jet and p_T^{truth} is the transverse momentum of the jet constructed from stable truth particles excluding muons and neutrinos. Stable particles are defined as those with a lifetime of 10 ps or more in the laboratory frame. The function is corrected using $\gamma + \text{jet}$ data events where the photon and the jet are balanced. These events are selected by a single photon trigger and require at least one signal photon and one baseline jet. To suppress soft radiation that would affect the p_T balance between the jet and the photon, the angle between the leading jet and the leading photon in the transverse plane is required to be larger than 2.9 rad, and the second-leading jet is required to have p_T of less than 20 % of the p_T of the photon. Using the p_T of the balanced photon as reference for that of the jet, the p_T response of jets is measured in data and MC. The jet energy resolution smearing function is then modified to match p_T response between data and MC. The method is validated by closure tests using MC simulation, and also using data in the $80 \text{ GeV} < E_T^{\text{miss}} < 160 \text{ GeV}$ region.

Other backgrounds

The estimation of other background processes producing two or three prompt leptons, such as diboson, triboson, $t\bar{t}V$, tZ or Wt production, is performed using the MC samples described in Sect. 3.

Since $t\bar{t}Z$ is the main background in the three-lepton SRs and has a topology very similar to a $\tilde{t}_2 \rightarrow Z\tilde{t}_1$ signal, dedicated validation regions with an enhanced contribution from this background and orthogonal to the SRs are defined to verify the MC prediction in data. These regions are defined requiring at least three leptons and the same $m_{\ell\ell}$ and b -jet requirements as the SRs. In order to enhance the $t\bar{t}Z$ contribution and reduce the possible contamination from signal events, the events are required to have from three to five jets with $p_T > 30 \text{ GeV}$ and fewer than five jets with $p_T > 50 \text{ GeV}$. The E_T^{miss} is required to be less than 150 GeV except for events with 5 jets with $p_T > 30 \text{ GeV}$ where the E_T^{miss} is required to be less than 60 GeV to avoid overlaps with the SRs. The third leading lepton is required to have $p_T > 20 \text{ GeV}$ to reduce the contribution from non-prompt leptons. Two separate validation regions are defined using the $p_T(\ell\ell)$ variable: VR3A with $p_T(\ell\ell) < 120 \text{ GeV}$ and VR3B with $p_T(\ell\ell) > 120 \text{ GeV}$. The contamination from a potential signal can be large in these validation regions but would typically affect VR3A and VR3B differently depend-

Table 3 Number of events in the VR3A and VR3B $t\bar{t}Z$ validation regions together with the expectation for some signal points in the \tilde{t}_2 simplified model. The errors on the backgrounds include both statistical and systematic uncertainties. Only statistical uncertainties are shown for the signal points

	VR3A	VR3B
Data	24	13
Total SM	19 ± 5	12.1 ± 3.2
MC exp. $t\bar{t}Z$	7.9 ± 2.1	5.9 ± 1.6
MC exp. tZ	2.7 ± 2.7	1.5 ± 1.5
Data-driven non-prompt	5.9 ± 2.9	2.7 ± 1.4
MC exp. diboson, triboson	1.5 ± 0.5	1.9 ± 0.6
MC exp. $t\bar{t}W$	0.35 ± 0.10	0.05 ± 0.02
MC exp. $Wh, Zh, t\bar{t}h$	0.3 ± 0.3	0.05 ± 0.05
$(m_{\tilde{t}_2}, m_{\tilde{\chi}_1^0}) = (500, 20) \text{ GeV}$	1.6 ± 0.6	7.5 ± 1.2
$(m_{\tilde{t}_2}, m_{\tilde{\chi}_1^0}) = (500, 120) \text{ GeV}$	3.3 ± 0.8	3.9 ± 0.8
$(m_{\tilde{t}_2}, m_{\tilde{\chi}_1^0}) = (550, 20) \text{ GeV}$	0.6 ± 0.3	4.6 ± 0.7
$(m_{\tilde{t}_2}, m_{\tilde{\chi}_1^0}) = (550, 220) \text{ GeV}$	2.7 ± 0.5	2.2 ± 0.5

ing on the \tilde{t}_2 - \tilde{t}_1 mass splitting. Table 3 shows the expected number of events in these validation regions taken from MC or data-driven estimations together with the observed number of events. The expected contribution from selected signal models is also shown. The $t\bar{t}Z$ contribution is 40–50 % of the total expected event count, and a good agreement with data is observed in both regions.

6 Systematic uncertainties

The dominant detector-related systematic effects are due to the jet energy scale (JES) and resolution (JER) uncertainties, and the uncertainties on the b -tagging efficiency and mistag rates.

The JES uncertainty is derived from a combination of simulation, test-beam data and in-situ measurements [74]. Additional terms accounting for flavour composition, flavour response, pile-up and b -jet scale uncertainties are taken into account. These uncertainties sum to 10–20 % of the total number of estimated background events depending on the SR. JER uncertainties are determined with an in-situ measurement of the jet response asymmetry in dijet events [89], and the impact on the SRs ranges between 1–10 %. Uncertainties associated with the b -tagging efficiency and mistagging of a c - and light-quark jet are obtained from the same techniques used in the derivation of their correction factors. The uncertainty on the expected number of background events in the SR due to b -tagging ranges between 4–10 %.

For the non-prompt lepton background estimation, uncertainties are assigned due to the statistical uncertainty on the

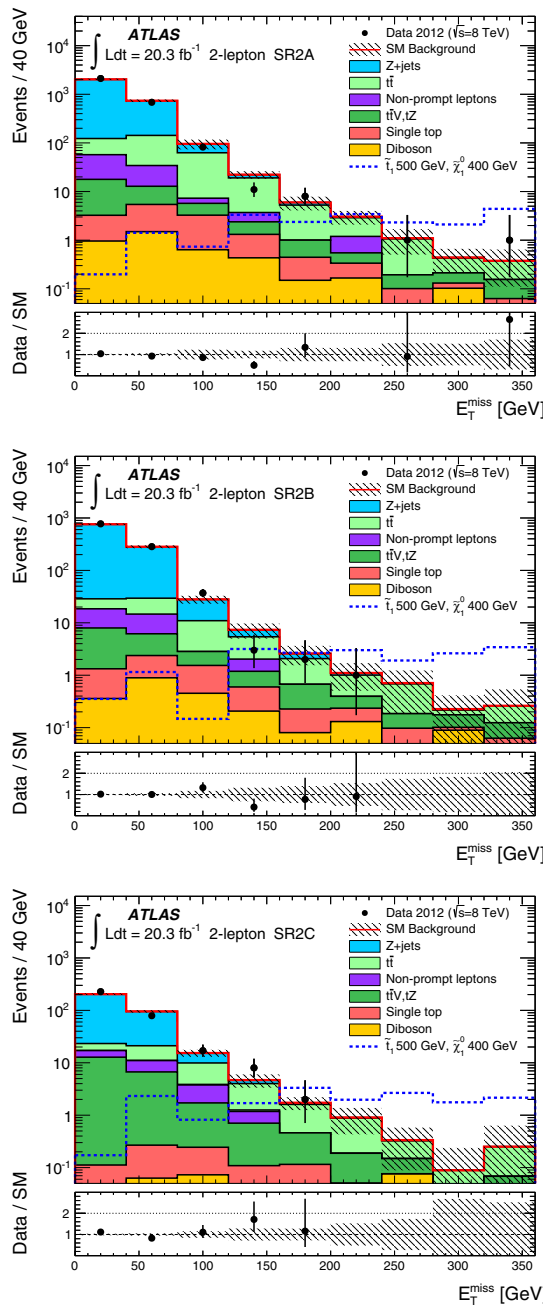


Fig. 2 The missing transverse momentum distribution for the 2-lepton SRs SR2A (top), SR2B (middle) and SR2C (bottom) before the final E_T^{miss} selection after the background fit. $Z + \text{jets}$ distributions are obtained using the jet smearing method. Shaded bands denote the statistical and systematic uncertainty on the background. For illustration, distributions for a GMSB signal scenario with $m_{\tilde{t}_1} = 500$ GeV, $m_{\tilde{\chi}_1^0} = 400$ GeV are shown. The last bin includes the histogram overflow

SR3B. For model-dependent interpretations, the fit described in Sect. 5 is modified to include the expected signal contamination of the CRs and the observed number of events in the SRs as well as an extra free parameter for a possible BSM signal strength which is constrained to be non-negative. The

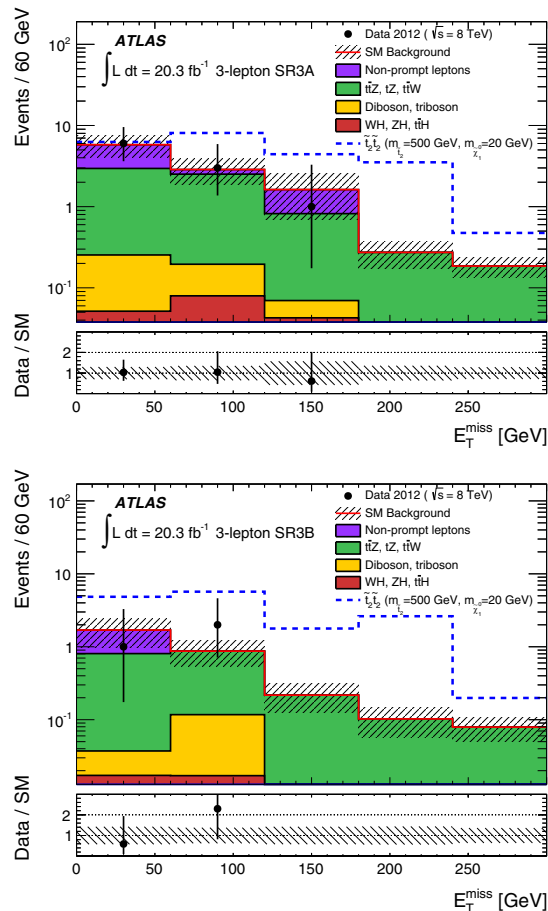


Fig. 3 The missing transverse momentum for the 3-lepton SRs SR3A (top) and SR3B (bottom) before the final E_T^{miss} selection. Shaded bands denote the statistical and systematic uncertainty on the background. For illustration, distributions for a signal point in the \tilde{t}_2 simplified model with $m_{\tilde{t}_2} = 500$ GeV and $m_{\tilde{\chi}_1^0} = 20$ GeV are also shown. The last bin includes the histogram overflow

Table 5 Signal model independent upper limits on the visible signal cross section ($\sigma_{\text{vis}} = \sigma_{\text{prod}} \times A \times \epsilon$) in the five SRs. The numbers (in parenthesis) give the observed (expected) 95 % CL upper limits. Calculations are performed with pseudo-experiments. The $\pm 1\sigma$ variations on the expected limit due to the statistical and background systematic uncertainties are also shown. The equivalent limits on the visible cross section calculated using an asymptotic method are given inside the square brackets

Signal region	σ_{vis} [fb]
SR2A	$0.40 (0.46^{+0.16}_{-0.13})$
SR2B	$0.19 (0.24^{+0.07}_{-0.05})$
SR2C	$0.20 (0.27^{+0.11}_{-0.07})$
SR3A	$0.30 (0.31^{+0.14}_{-0.05})$
SR3B	$0.26 (0.20^{+0.08}_{-0.02})$

expected and observed exclusion limits are calculated using asymptotic formulae for each SUSY model point, taking into account the theoretical and experimental uncertainties on the

SM background and the experimental uncertainties on the signal. The impact of the uncertainties on the signal cross section is also addressed for the observed limit only by show-

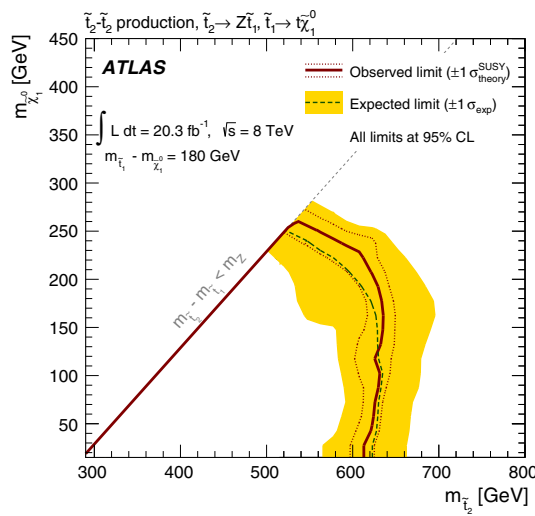
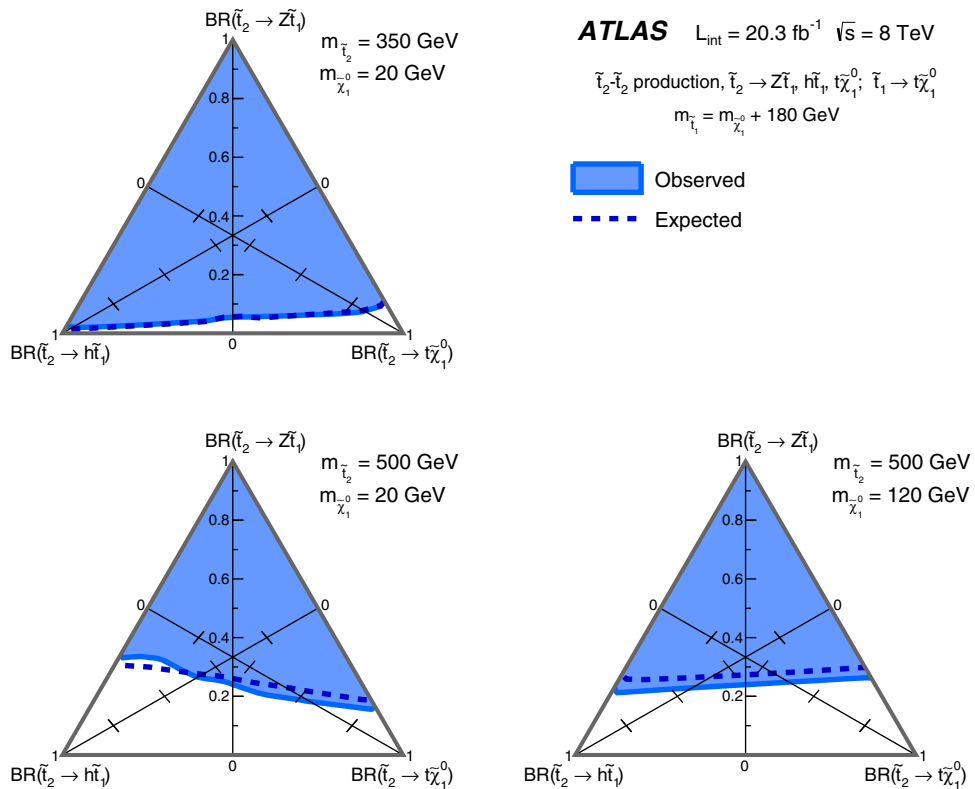


Fig. 4 Expected and observed exclusion limits in the $m_{\tilde{t}_2}$ - $m_{\tilde{\chi}_1^0}$ plane for the direct \tilde{t}_2 pair production simplified model with $\text{BR}(\tilde{t}_2 \rightarrow Z\tilde{t}_1) = 1$. The contours of the band around the expected limit are the $\pm 1\sigma$ results, including all uncertainties except theoretical uncertainties on the signal cross section. The dotted lines around the observed limit illustrate the change in the observed limit as the nominal signal cross section is scaled up and down by the theoretical uncertainty. All limits are computed at 95 % CL

Fig. 5 Exclusion limits at 95 % CL are shown for the direct \tilde{t}_2 pair production simplified model as a function of the branching ratios $\text{BR}(\tilde{t}_2 \rightarrow Z\tilde{t}_1)$, $\text{BR}(\tilde{t}_2 \rightarrow h\tilde{t}_1)$ and $\text{BR}(\tilde{t}_2 \rightarrow t\tilde{\chi}_1^0)$ for $(m_{\tilde{t}_2}, m_{\tilde{\chi}_1^0}) = (350, 20)$ GeV (top), $(500, 20)$ GeV (bottom left) and $(500, 120)$ GeV (bottom right). The dashed and solid lines show the expected and observed limits, respectively, including all uncertainties except the theoretical signal cross section uncertainty (PDF and scale)



ing the results obtained when moving the nominal cross section up or down by the $\pm 1\sigma$ theoretical uncertainty. Quoted numerical limits on the particle masses refer to the signal cross sections reduced by 1σ .

Figure 4 shows the limit obtained in the \tilde{t}_2 simplified model, which excludes $m_{\tilde{t}_2} < 525$ GeV for $m_{\tilde{\chi}_1^0} < 240$ GeV and $m_{\tilde{t}_2} < 600$ GeV for $m_{\tilde{\chi}_1^0} < 200$ GeV. The interpolation of the limit contours between the simulated points towards the $\tilde{t}_2 \rightarrow Z\tilde{t}_1$ kinematic boundary has been established using MC generator level information. A reduction in acceptance of up to 20 % is observed in the region where $m_{\tilde{t}_2} - m_{\tilde{t}_1} - m_Z$ is comparable to the Z boson width. The region with $m_{\tilde{t}_2} - m_{\tilde{t}_1} < m_Z$, where the $\tilde{t}_2 \rightarrow Z^{(*)}\tilde{t}_1$ decay involves an off-shell Z , has not been considered since in that case other \tilde{t}_2 decay modes, such as $\tilde{t}_2 \rightarrow t\tilde{\chi}_1^0$, would be dominant. If the assumption on the 100 % branching ratio for the $\tilde{t}_2 \rightarrow Z\tilde{t}_1$ decay mode is relaxed, the \tilde{t}_2 can also decay via $\tilde{t}_2 \rightarrow h\tilde{t}_1$ and $\tilde{t}_2 \rightarrow t\tilde{\chi}_1^0$. Exclusion limits as a function of the \tilde{t}_2 branching ratios are shown in Fig. 5 for representative values of the masses of \tilde{t}_2 and $\tilde{\chi}_1^0$. For low \tilde{t}_2 mass ($m_{\tilde{t}_2} = 350$ GeV), SUSY models with $\text{BR}(\tilde{t}_2 \rightarrow Z\tilde{t}_1)$ above 10 % are excluded. For higher stop mass ($m_{\tilde{t}_2} = 500$ GeV), models with $\text{BR}(\tilde{t}_2 \rightarrow Z\tilde{t}_1)$ above 15–30 % are excluded, with a small dependence on the value of the neutralino mass, $\text{BR}(\tilde{t}_2 \rightarrow h\tilde{t}_1)$ and $\text{BR}(\tilde{t}_2 \rightarrow t\tilde{\chi}_1^0)$.

In Fig. 6 the expected and observed limits are shown for the GMSB scenarios on the \tilde{t}_1 , $\tilde{\chi}_1^0$ mass plane. Stop

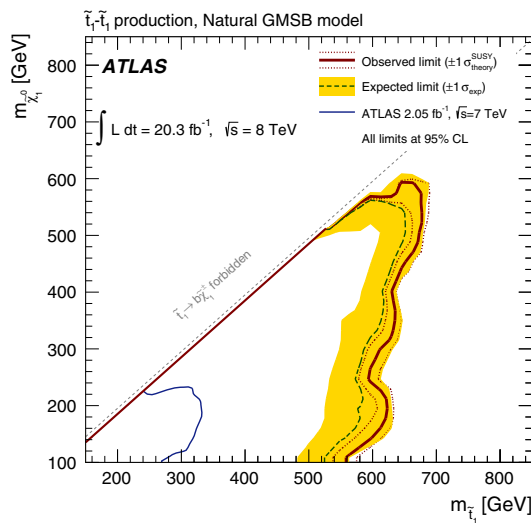


Fig. 6 Expected and observed exclusion limits at 95 % CL for the stop natural GMSB model described in the text. The contours of the band around the expected limit are the $\pm 1\sigma$ results, including all uncertainties except theoretical uncertainties on the signal cross section. The dotted lines around the observed limit illustrate the change in the observed limit as the nominal signal cross section is scaled up and down by the theoretical uncertainty. For comparison, the observed exclusion limit with 2.05 fb^{-1} of data at $\sqrt{s} = 7 \text{ TeV}$ at ATLAS for a similar model [34] is shown

masses up to 540 GeV are excluded for neutralino masses of $100 \text{ GeV} < m_{\tilde{\chi}_1^0} < m_{\tilde{t}_1} - 10 \text{ GeV}$. In the parameter space region where the \tilde{t}_1 only decays via $b\tilde{\chi}_1^\pm$, the exclusion extends up to stop masses of 660 GeV for neutralinos of 550 GeV. For illustration, the exclusion limits obtained with 2.05 fb^{-1} of ATLAS data at $\sqrt{s} = 7 \text{ TeV}$ for the similar model are also shown, in which the maximum limit on the stop masses was 330 GeV. Due to the increase in statistics and the proton–proton collision energy, as well as the optimised selections for these conditions, much stronger constraints are now set on this model.

8 Summary and Conclusions

This paper presents a dedicated search for direct stop pair production in decays with an experimental signature compatible with the production of a Z boson, b -jets and missing transverse momentum. The analysis is performed with pp collision data at $\sqrt{s} = 8 \text{ TeV}$ collected with the ATLAS detector at the LHC corresponding to an integrated luminosity of 20.3 fb^{-1} . The results are interpreted in the framework of simplified models with production of \tilde{t}_2 as well as in a natural GMSB model.

In a simplified model characterised by the decay chain $\tilde{t}_2 \rightarrow Z\tilde{t}_1$ with $\tilde{t}_1 \rightarrow t\tilde{\chi}_1^0$ and the mass difference between \tilde{t}_1 and $\tilde{\chi}_1^0$ slightly larger than the top mass, parameter space regions with $m_{\tilde{t}_2} < 600 \text{ GeV}$ and $m_{\tilde{\chi}_1^0} < 200 \text{ GeV}$ are

excluded at 95 % CL. When the $\tilde{t}_2 \rightarrow h\tilde{t}_1$ and $\tilde{t}_2 \rightarrow t\tilde{\chi}_1^0$ decays are included in the model, $\text{BR}(\tilde{t}_2 \rightarrow Z\tilde{t}_1) > 10\text{--}30\%$ are excluded for several mass configurations. These are the first experimental results on the search for \tilde{t}_2 .

In the GMSB scenario, where the \tilde{t}_1 might decay to $b\tilde{\chi}_1^\pm$ or $t\tilde{\chi}_1^0(\tilde{\chi}_2^0)$ and the $\tilde{\chi}_1^0$ decay in $Z\tilde{G}$ or $h\tilde{G}$, parameter space regions with \tilde{t}_1 masses below 540 GeV are excluded at 95 % CL for $100 \text{ GeV} < m_{\tilde{\chi}_1^0} < m_{\tilde{t}_1} - 10 \text{ GeV}$. These limits are much stronger than those set on the similar model considered in the search at $\sqrt{s} = 7 \text{ TeV}$. For $\tilde{\chi}_1^0$ masses of about 550 GeV, better sensitivity is achieved and \tilde{t}_1 masses below 660 GeV are excluded.

Acknowledgments We thank CERN for the very successful operation of the LHC, as well as the support staff from our institutions without whom ATLAS could not be operated efficiently. We acknowledge the support of ANPCyT, Argentina; YerPhI, Armenia; ARC, Australia; BMWF and FWF, Austria; ANAS, Azerbaijan; SSTC, Belarus; CNPq and FAPESP, Brazil; NSERC, NRC and CFI, Canada; CERN; CONICYT, Chile; CAS, MOST and NSFC, China; COLCIENCIAS, Colombia; MSMT CR, MPO CR and VSC CR, Czech Republic; DNRF, DNSRC and Lundbeck Foundation, Denmark; EPLANET, ERC and NSRF, European Union; IN2P3-CNRS, CEA-DSM/IRFU, France; GNSF, Georgia; BMBF, DFG, HGF, MPG and AvH Foundation, Germany; GSRT and NSRF, Greece; ISF, MINERVA, GIF, I-CORE and Benoziyo Center, Israel; INFN, Italy; MEXT and JSPS, Japan; CNRST, Morocco; FOM and NWO, Netherlands; BRF and RCN, Norway; MNiSW and NCN, Poland; GRICES and FCT, Portugal; MNE/IFA, Romania; MES of Russia and ROSATOM, Russian Federation; JINR; MSTD, Serbia; MSSR, Slovakia; ARRS and MIZŠ, Slovenia; DST/NRF, South Africa; MINECO, Spain; SRC and Wallenberg Foundation, Sweden; SER, SNSF and Cantons of Bern and Geneva, Switzerland; NSC, Taiwan; TAEK, Turkey; STFC, the Royal Society and Leverhulme Trust, UK; DOE and NSF, USA. The crucial computing support from all WLCG partners is acknowledged gratefully, in particular from CERN and the ATLAS Tier-1 facilities at TRIUMF (Canada), NDGF (Denmark, Norway, Sweden), CC-IN2P3 (France), KIT/GridKA (Germany), INFN-CNAF (Italy), NL-T1 (Netherlands), PIC (Spain), ASGC (Taiwan), RAL (UK) and BNL (USA) and in the Tier-2 facilities worldwide.

Open Access This article is distributed under the terms of the Creative Commons Attribution License which permits any use, distribution, and reproduction in any medium, provided the original author(s) and the source are credited.

Funded by SCOAP³ / License Version CC BY 4.0.

References

1. H. Miyazawa, Prog. Theor. Phys. **36**(6), 1266–1276 (1966)
2. P. Ramond, Phys. Rev. D **3**, 2415–2418 (1971)
3. Y. Gol'fand, E. Likhtman, JETP Lett. **13**, 323–326 (1971)
4. A. Neveu, J.H. Schwarz, Nucl. Phys. B **31**, 86–112 (1971)
5. A. Neveu, J.H. Schwarz, Phys. Rev. D **4**, 1109–1111 (1971)
6. J. Gervais, B. Sakita, Nucl. Phys. B **34**, 632–639 (1971)
7. D. Volkov, V. Akulov, Phys. Lett. B **46**, 109–110 (1973)
8. J. Wess, B. Zumino, Phys. Lett. B **49**, 52 (1974)
9. J. Wess, B. Zumino, Nucl. Phys. B **70**, 39–50 (1974)
10. P. Fayet, Phys. Lett. B **64**, 159 (1976)
11. P. Fayet, Phys. Lett. B **69**, 489 (1977)

- ³⁴ Laboratoire de Physique Corpusculaire, Clermont Université and Université Blaise Pascal and CNRS/IN2P3, Clermont-Ferrand, France
- ³⁵ Nevis Laboratory, Columbia University, Irvington, NY, USA
- ³⁶ Niels Bohr Institute, University of Copenhagen, Kobenhavn, Denmark
- ³⁷ INFN Gruppo Collegato di Cosenza, Laboratori Nazionali di Frascati, Frascati, Italy
- ³⁸ AGH University of Science and Technology, Faculty of Physics and Applied Computer Science, Kraków, Poland
- ³⁹ The Henryk Niewodniczanski Institute of Nuclear Physics, Polish Academy of Sciences, Kraków, Poland
- ⁴⁰ Physics Department, Southern Methodist University, Dallas, TX, USA
- ⁴¹ Physics Department, University of Texas at Dallas, Richardson, TX, USA
- ⁴² DESY, Hamburg and Zeuthen, Berlin, Germany
- ⁴³ Institut für Experimentelle Physik IV, Technische Universität Dortmund, Dortmund, Germany
- ⁴⁴ Institut für Kern- und Teilchenphysik, Technische Universität Dresden, Dresden, Germany
- ⁴⁵ Department of Physics, Duke University, Durham, NC, USA
- ⁴⁶ SUPA, School of Physics and Astronomy, University of Edinburgh, Edinburgh, UK
- ⁴⁷ INFN Laboratori Nazionali di Frascati, Frascati, Italy
- ⁴⁸ Fakultät für Mathematik und Physik, Albert-Ludwigs-Universität, Freiburg, Germany
- ⁴⁹ Section de Physique, Université de Genève, Geneva, Switzerland
- ⁵⁰ INFN Sezione di Genova, Genoa, Italy
- ⁵¹ E. Andronikashvili Institute of Physics, Iv. Javakhishvili Tbilisi State University, Tbilisi, Georgia
- ⁵² II Physikalisch Institut, Justus-Liebig-Universität Giessen, Giessen, Germany
- ⁵³ SUPA, School of Physics and Astronomy, University of Glasgow, Glasgow, UK
- ⁵⁴ II Physikalisch Institut, Georg-August-Universität, Göttingen, Germany
- ⁵⁵ Laboratoire de Physique Subatomique et de Cosmologie, Université Grenoble-Alpes, CNRS/IN2P3 Grenoble, France
- ⁵⁶ Department of Physics, Hampton University, Hampton, VA, USA
- ⁵⁷ Laboratory for Particle Physics and Cosmology, Harvard University, Cambridge, MA, USA
- ⁵⁸ Kirchhoff-Institut für Physik, Ruprecht-Karls-Universität Heidelberg, Heidelberg, Germany
- ⁵⁹ Faculty of Applied Information Science, Hiroshima Institute of Technology, Hiroshima, Japan
- ⁶⁰ Department of Physics, Indiana University, Bloomington, IN, USA
- ⁶¹ Institut für Astro- und Teilchenphysik, Leopold-Franzens-Universität, Innsbruck, Austria
- ⁶² University of Iowa, Iowa City, IA, USA
- ⁶³ Department of Physics and Astronomy, Iowa State University, Ames, IA, USA
- ⁶⁴ Joint Institute for Nuclear Research, JINR Dubna, Dubna, Russia
- ⁶⁵ KEK, High Energy Accelerator Research Organization, Tsukuba, Japan
- ⁶⁶ Graduate School of Science, Kobe University, Kobe, Japan
- ⁶⁷ Faculty of Science, Kyoto University, Kyoto, Japan
- ⁶⁸ Kyoto University of Education, Kyoto, Japan
- ⁶⁹ Department of Physics, Kyushu University, Fukuoka, Japan
- ⁷⁰ Instituto de Física La Plata, Universidad Nacional de La Plata and CONICET, La Plata, Argentina
- ⁷¹ Physics Department, Lancaster University, Lancaster, UK
- ⁷² INFN Sezione di Lecce, Lecce, Italy
- ⁷³ Oliver Lodge Laboratory, University of Liverpool, Liverpool, UK
- ⁷⁴ Department of Physics, Jožef Stefan Institute and University of Ljubljana, Ljubljana, Slovenia
- ⁷⁵ School of Physics and Astronomy, Queen Mary University of London, London, UK
- ⁷⁶ Department of Physics, Royal Holloway University of London, Surrey, UK
- ⁷⁷ Department of Physics and Astronomy, University College London, London, UK
- ⁷⁸ Louisiana Tech University, Ruston, LA, USA
- ⁷⁹ Laboratoire de Physique Nucléaire et de Hautes Energies, UPMC and Université Paris-Diderot and CNRS/IN2P3, Paris, France
- ⁸⁰ Fysiska institutionen, Lunds universitet, Lund, Sweden
- ⁸¹ Departamento de Fisica Teorica C-15, Universidad Autonoma de Madrid, Madrid, Spain
- ⁸² Institut für Physik, Universität Mainz, Mainz, Germany
- ⁸³ School of Physics and Astronomy, University of Manchester, Manchester, UK
- ⁸⁴ CPPM, Aix-Marseille Université and CNRS/IN2P3, Marseille, France

- ⁸⁵ Department of Physics, University of Massachusetts, Amherst, MA, USA
⁸⁶ Department of Physics, McGill University, Montreal, QC, Canada
⁸⁷ School of Physics, University of Melbourne, Melbourne, VIC, Australia
⁸⁸ Department of Physics, The University of Michigan, Ann Arbor, MI, USA
⁸⁹ Department of Physics and Astronomy, Michigan State University, East Lansing, MI, USA
⁹⁰ INFN Sezione di Milano, Milan, Italy
⁹¹ B.I. Stepanov Institute of Physics, National Academy of Sciences of Belarus, Minsk, Republic of Belarus
⁹² National Scientific and Educational Centre for Particle and High Energy Physics, Minsk, Republic of Belarus
⁹³ Department of Physics, Massachusetts Institute of Technology, Cambridge, MA, USA
⁹⁴ Group of Particle Physics, University of Montreal, Montreal, QC, Canada
⁹⁵ P.N. Lebedev Institute of Physics, Academy of Sciences, Moscow, Russia
⁹⁶ Institute for Theoretical and Experimental Physics (ITEP), Moscow, Russia
⁹⁷ Moscow Engineering and Physics Institute (MEPhI), Moscow, Russia
⁹⁸ D.V. Skobeltsyn Institute of Nuclear Physics, M.V. Lomonosov Moscow State University, Moscow, Russia
⁹⁹ Fakultät für Physik, Ludwig-Maximilians-Universität München, Munich, Germany
¹⁰⁰ Max-Planck-Institut für Physik (Werner-Heisenberg-Institut), Munich, Germany
¹⁰¹ Nagasaki Institute of Applied Science, Nagasaki, Japan
¹⁰² Graduate School of Science and Kobayashi-Maskawa Institute, Nagoya University, Nagoya, Japan
¹⁰³ INFN Sezione di Napoli, Naples, Italy
¹⁰⁴ Department of Physics and Astronomy, University of New Mexico, Albuquerque, NM, USA
¹⁰⁵ Institute for Mathematics, Astrophysics and Particle Physics, Radboud University Nijmegen/Nikhef, Nijmegen, The Netherlands
¹⁰⁶ Nikhef National Institute for Subatomic Physics and University of Amsterdam, Amsterdam, The Netherlands
¹⁰⁷ Department of Physics, Northern Illinois University, DeKalb, IL, USA
¹⁰⁸ Budker Institute of Nuclear Physics, SB RAS, Novosibirsk, Russia
¹⁰⁹ Department of Physics, New York University, New York, NY, USA
¹¹⁰ Ohio State University, Columbus, OH, USA
¹¹¹ Faculty of Science, Okayama University, Okayama, Japan
¹¹² Homer L. Dodge Department of Physics and Astronomy, University of Oklahoma, Norman, OK, USA
¹¹³ Department of Physics, Oklahoma State University, Stillwater, OK, USA
¹¹⁴ Palacký University, RCPTM, Olomouc, Czech Republic
¹¹⁵ Center for High Energy Physics, University of Oregon, Eugene, OR, USA
¹¹⁶ LAL, Université Paris-Sud and CNRS/IN2P3, Orsay, France
¹¹⁷ Graduate School of Science, Osaka University, Osaka, Japan
¹¹⁸ Department of Physics, University of Oslo, Oslo, Norway
¹¹⁹ Department of Physics, Oxford University, Oxford, UK
¹²⁰ INFN Sezione di Pavia, Pavia, Italy
¹²¹ Department of Physics, University of Pennsylvania, Philadelphia, PA, USA
¹²² Petersburg Nuclear Physics Institute, Gatchina, Russia
¹²³ INFN Sezione di Pisa, Pisa, Italy
¹²⁴ Department of Physics and Astronomy, University of Pittsburgh, Pittsburgh, PA, USA
¹²⁵ Laboratorio de Instrumentacao e Fisica Experimental de Particulas, LIP, Lisbon, Portugal
¹²⁶ Institute of Physics, Academy of Sciences of the Czech Republic, Praha, Czech Republic
¹²⁷ Czech Technical University in Prague, Praha, Czech Republic
¹²⁸ Faculty of Mathematics and Physics, Charles University in Prague, Praha, Czech Republic
¹²⁹ State Research Center Institute for High Energy Physics, Protvino, Russia
¹³⁰ Particle Physics Department, Rutherford Appleton Laboratory, Didcot, UK
¹³¹ Physics Department, University of Regina, Regina, SK, Canada
¹³² Ritumeikan University, Kusatsu, Shiga, Japan
¹³³ INFN Sezione di Roma, Rome, Italy
¹³⁴ INFN Sezione di Roma Tor Vergata, Rome, Italy
¹³⁵ INFN Sezione di Roma Tre, Rome, Italy

- ¹³⁶ Faculté des Sciences Ain Chock, Réseau Universitaire de Physique des Hautes Energies, Université Hassan II, Casablanca, Morocco
- ¹³⁷ DSM/IRFU (Institut de Recherches sur les Lois Fondamentales de l'Univers), CEA Saclay (Commissariat à l'Energie Atomique et aux Energies Alternatives), Gif-sur-Yvette, France
- ¹³⁸ Santa Cruz Institute for Particle Physics, University of California Santa Cruz, Santa Cruz, CA, USA
- ¹³⁹ Department of Physics, University of Washington, Seattle, WA, USA
- ¹⁴⁰ Department of Physics and Astronomy, University of Sheffield, Sheffield, UK
- ¹⁴¹ Department of Physics, Shinshu University, Nagano, Japan
- ¹⁴² Fachbereich Physik, Universität Siegen, Siegen, Germany
- ¹⁴³ Department of Physics, Simon Fraser University, Burnaby, BC, Canada
- ¹⁴⁴ SLAC National Accelerator Laboratory, Stanford, CA, USA
- ¹⁴⁵ Faculty of Mathematics, Physics and Informatics, Comenius University, Bratislava, Slovakia
- ¹⁴⁶ Department of Physics, University of Cape Town, Cape Town, South Africa
- ¹⁴⁷ Department of Physics, Stockholm University, Stockholm, Sweden
- ¹⁴⁸ Physics Department, Royal Institute of Technology, Stockholm, Sweden
- ¹⁴⁹ Departments of Physics and Astronomy and Chemistry, Stony Brook University, Stony Brook, NY, USA
- ¹⁵⁰ Department of Physics and Astronomy, University of Sussex, Brighton, UK
- ¹⁵¹ School of Physics, University of Sydney, Sydney, Australia
- ¹⁵² Institute of Physics, Academia Sinica, Taipei, Taiwan
- ¹⁵³ Department of Physics, Technion: Israel Institute of Technology, Haifa, Israel
- ¹⁵⁴ Raymond and Beverly Sackler School of Physics and Astronomy, Tel Aviv University, Tel Aviv, Israel
- ¹⁵⁵ Department of Physics, Aristotle University of Thessaloniki, Thessaloniki, Greece
- ¹⁵⁶ International Center for Elementary Particle Physics and Department of Physics, The University of Tokyo, Tokyo, Japan
- ¹⁵⁷ Graduate School of Science and Technology, Tokyo Metropolitan University, Tokyo, Japan
- ¹⁵⁸ Department of Physics, Tokyo Institute of Technology, Tokyo, Japan
- ¹⁵⁹ Department of Physics, University of Toronto, Toronto, ON, Canada
- ¹⁶⁰ TRIUMF, Vancouver, BC, Canada
- ¹⁶¹ Faculty of Pure and Applied Sciences, University of Tsukuba, Tsukuba, Japan
- ¹⁶² Department of Physics and Astronomy, Tufts University, Medford, MA, USA
- ¹⁶³ Centro de Investigaciones, Universidad Antonio Narino, Bogota, Colombia
- ¹⁶⁴ Department of Physics and Astronomy, University of California Irvine, Irvine, CA, USA
- ¹⁶⁵ INFN Gruppo Collegato di Udine, Sezione di Trieste, Udine, Italy
- ¹⁶⁶ Department of Physics, University of Illinois, Urbana, IL, USA
- ¹⁶⁷ Department of Physics and Astronomy, University of Uppsala, Uppsala, Sweden
- ¹⁶⁸ Instituto de Física Corpuscular (IFIC) and Departamento de Física Atómica, Molecular y Nuclear and Departamento de Ingeniería Electrónica and Instituto de Microelectrónica de Barcelona (IMB-CNM), University of Valencia and CSIC, Valencia, Spain
- ¹⁶⁹ Department of Physics, University of British Columbia, Vancouver, BC, Canada
- ¹⁷⁰ Department of Physics and Astronomy, University of Victoria, Victoria, BC, Canada
- ¹⁷¹ Department of Physics, University of Warwick, Coventry, USA
- ¹⁷² Waseda University, Tokyo, Japan
- ¹⁷³ Department of Particle Physics, The Weizmann Institute of Science, Rehovot, Israel
- ¹⁷⁴ Department of Physics, University of Wisconsin, Madison, WI, USA
- ¹⁷⁵ Fakultät für Physik und Astronomie, Julius-Maximilians-Universität, Würzburg, Germany
- ¹⁷⁶ Fachbereich C Physik, Bergische Universität Wuppertal, Wuppertal, Germany
- ¹⁷⁷ Department of Physics, Yale University, New Haven, CT, USA
- ¹⁷⁸ Yerevan Physics Institute, Yerevan, Armenia
- ¹⁷⁹ Centre de Calcul de l'Institut National de Physique Nucléaire et de Physique des Particules (IN2P3), Villeurbanne, France
- ¹⁸⁰ Department of Physics, Gazi University, Ankara, Turkey
- ¹⁸¹ Division of Physics, TOBB University of Economics and Technology, Ankara, Turkey
- ¹⁸² Turkish Atomic Energy Authority, Ankara, Turkey
- ¹⁸³ Vinca Institute of Nuclear Sciences, University of Belgrade, Belgrade, Serbia
- ¹⁸⁴ Department of Physics, Dogus University, Istanbul, Turkey

- ¹⁸⁵ Department of Physics Engineering, Gaziantep University, Gaziantep, Turkey
¹⁸⁶ Dipartimento di Fisica e Astronomia, Università di Bologna, Bologna, Italy
¹⁸⁷ Federal University of Juiz de Fora (UFJF), Juiz de Fora, Brazil
¹⁸⁸ Federal University of São João del Rei (UFSJ), São João del Rei, Brazil
¹⁸⁹ Instituto de Física, Universidade de São Paulo, São Paulo, Brazil
¹⁹⁰ National Institute for Research and Development of Isotopic and Molecular Technologies, Physics Department, Cluj-Napoca, Romania
¹⁹¹ University Politehnica Bucharest, Bucharest, Romania
¹⁹² West University in Timisoara, Timisoara, Romania
¹⁹³ Departamento de Física, Universidad Técnica Federico Santa María, Valparaíso, Chile
¹⁹⁴ Department of Modern Physics, University of Science and Technology of China, Anhui, China
¹⁹⁵ Department of Physics, Nanjing University, Jiangsu, China
¹⁹⁶ School of Physics, Shandong University, Shandong, China
¹⁹⁷ Physics Department, Shanghai Jiao Tong University, Shanghai, China
¹⁹⁸ Dipartimento di Fisica, Università della Calabria, Rende, Italy
¹⁹⁹ Marian Smoluchowski Institute of Physics, Jagiellonian University, Kraków, Poland
²⁰⁰ Dipartimento di Fisica, Università di Genova, Genoa, Italy
²⁰¹ High Energy Physics Institute, Tbilisi State University, Tbilisi, Georgia
²⁰² Physikalisches Institut, Ruprecht-Karls-Universität Heidelberg, Heidelberg, Germany
²⁰³ ZITI Institut für technische Informatik, Ruprecht-Karls-Universität Heidelberg, Mannheim, Germany
²⁰⁴ Dipartimento di Matematica e Fisica, Università del Salento, Lecce, Italy
²⁰⁵ Dipartimento di Fisica, Università di Milano, Milan, Italy
²⁰⁶ Dipartimento di Fisica, Università di Napoli, Naples, Italy
²⁰⁷ Dipartimento di Fisica, Università di Pavia, Pavia, Italy
²⁰⁸ Dipartimento di Fisica E. Fermi, Università di Pisa, Pisa, Italy
²⁰⁹ Faculdade de Ciências, Universidade de Lisboa, Lisbon, Portugal
²¹⁰ Department of Physics, University of Coimbra, Coimbra, Portugal
²¹¹ Centro de Física Nuclear da Universidade de Lisboa, Lisbon, Portugal
²¹² Departamento de Fisica, Universidade do Minho, Braga, Portugal
²¹³ Departamento de Fisica Teorica y del Cosmos and CAFPE, Universidad de Granada, Granada, Spain
²¹⁴ Dep Fisica and CEFITEC of Faculdade de Ciencias e Tecnologia, Universidade Nova de Lisboa, Caparica, Portugal
²¹⁵ Dipartimento di Fisica, Sapienza Università di Roma, Rome, Italy
²¹⁶ Dipartimento di Fisica, Università di Roma Tor Vergata, Rome, Italy
²¹⁷ Dipartimento di Matematica e Fisica, Università Roma Tre, Rome, Italy
²¹⁸ Centre National de l'Energie des Sciences Techniques Nucleaires, Rabat, Morocco
²¹⁹ Faculté des Sciences Semlalia, Université Cadi Ayyad, LPHEA-Marrakech, Marrakesh, Morocco
²²⁰ Faculté des Sciences, Université Mohamed Premier and LPTPM, Oujda, Morocco
²²¹ Faculté des sciences, Université Mohammed V-Agdal, Rabat, Morocco
²²² Department of Subnuclear Physics, Institute of Experimental Physics of the Slovak Academy of Sciences, Kosice, Slovak Republic
²²³ Department of Physics, University of Johannesburg, Johannesburg, South Africa
²²⁴ School of Physics, University of the Witwatersrand, Johannesburg, South Africa
²²⁵ The Oskar Klein Centre, Stockholm, Sweden
²²⁶ Department of Physics and Astronomy, York University, Toronto, ON, Canada
²²⁷ ICTP, Trieste, Italy
²²⁸ Dipartimento di Chimica, Fisica e Ambiente, Università di Udine, Udine, Italy

^a Also at Department of Physics, King's College London, London, UK

^b Also at Institute of Physics, Azerbaijan Academy of Sciences, Baku, Azerbaijan

^c Also at Particle Physics Department, Rutherford Appleton Laboratory, Didcot, UK

^d Also at TRIUMF, Vancouver BC, Canada

^e Also at Department of Physics, California State University, Fresno CA, USA

^f Also at Novosibirsk State University, Novosibirsk, Russia

- ^g Also at CPPM, Aix-Marseille Université and CNRS/IN2P3, Marseille, France
^h Also at Università di Napoli Parthenope, Naples, Italy
ⁱ Also at Institute of Particle Physics (IPP), Victoria, Canada
^j Also at Department of Physics, St. Petersburg State Polytechnical University, St. Petersburg, Russia
^k Also at Department of Financial and Management Engineering, University of the Aegean, Chios, Greece
^l Also at Louisiana Tech University, Ruston, LA, USA
^m Also at Institutio Catalana de Recerca i Estudis Avancats, ICREA, Barcelona, Spain
ⁿ Also at CERN, Geneva, Switzerland
^o Also at Ochadai Academic Production, Ochanomizu University, Tokyo, Japan
^p Also at Manhattan College, New York, NY, USA
^q Also at Institute of Physics, Academia Sinica, Taipei, Taiwan
^r Also at LAL, Université Paris-Sud and CNRS/IN2P3, Orsay, France
^s Also at School of Physics and Engineering, Sun Yat-sen University, Guangzhou, China
^t Also at Academia Sinica Grid Computing, Institute of Physics, Academia Sinica, Taipei, Taiwan
^u Also at Laboratoire de Physique Nucléaire et de Hautes Energies, UPMC and Université Paris-Diderot and CNRS/IN2P3, Paris, France
^v Also at School of Physical Sciences, National Institute of Science Education and Research, Bhubaneswar, India
^w Also at Dipartimento di Fisica, Sapienza Università di Roma, Rome, Italy
^x Also at Moscow Institute of Physics and Technology State University, Dolgoprudny, Russia
^y Also at Section de Physique, Université de Genève, Geneva, Switzerland
^z Also at Department of Physics, The University of Texas at Austin, Austin, TX, USA
^{aa} Also at Institute for Particle and Nuclear Physics, Wigner Research Centre for Physics, Budapest, Hungary
^{ab} Also at International School for Advanced Studies (SISSA), Trieste, Italy
^{ac} Also at Department of Physics and Astronomy, University of South Carolina, Columbia, SC, USA
^{ad} Also at Faculty of Physics, M.V. Lomonosov Moscow State University, Moscow, Russia
^{ae} Also at Physics Department, Brookhaven National Laboratory, Upton, NY, USA
^{af} Also at Moscow Engineering and Physics Institute (MEPhI), Moscow, Russia
^{ag} Also at Department of Physics, Oxford University, Oxford, UK
^{ah} Also at Department of Physics, Nanjing University, Jiangsu, China
^{ai} Also at Institut für Experimentalphysik, Universität Hamburg, Hamburg, Germany
^{aj} Also at Department of Physics, The University of Michigan, Ann Arbor, MI, USA
^{ak} Also at Discipline of Physics, University of KwaZulu-Natal, Durban, South Africa

*Deceased